Incorporation of a Binary Alloy in an Oxide Matrix via Single Source Precursor CVD Process

Michael Veith,*,† Nicolas Lecerf,† Sanjay Mathur,† Hao Shen,‡ and Stefan Hüfner‡

Institute of Inorganic Chemistry and Institute of Experimental Physics, University of Saarland, D-66041 Saarbrücken, Germany

Received March 15, 1999. Revised Manuscript Received August 25, 1999

Using a Ni−Sn heterometal alkoxide, $[Ni_2Sn_2(O^tBu)_8]$, in a chemical vapor deposition (CVD) process, thin films of biphasic composite, Ni_3Sn_4/SnO_2, have been obtained. Due to the presence of two metal atoms in a single molecule, the decomposition occurs at a molecular level resulting in *homogeneous incorporation of intermetallic Ni_3Sn_4 in an SnO_2 matrix*. The CVD experiments performed at different temperatures (450−550 °C) show that the obtained composite results from two chemical processes: (i) disproportionation of Sn(II) species and (ii) the redox reactions ocurring between Sn(II) and Ni(II) species. Fragmentation of the precursor and disproportionation of the tin(II) component dominate up to 500 °C, resulting in the formation of NiO, Sn(0), and SnO_2. Redox reactions are favored at higher temperature (550 °C) which lead to the formation of the Ni_3Sn_4 alloy. This alloy−metal oxide composite has been deposited on different substrates (steel, copper, silicon wafer), and no heterogeneity was observed on a micrometer level (energy-dispersive X-ray analysis). Powder X-ray diffraction patterns of the deposits obtained at 550 °C show Ni_3Sn_4 and SnO_2 as the only crystalline phases. The scanning electron micrograph images reveal a microstructured surface with a fibrous morphology. High-resolution transmission electron microscope investigations show a bimodal mixture where the Ni_3Sn_4 crystallites (ca. 60−80 nm) are uniformly dispersed in a SnO_2 matrix (30−45 nm). Well-developed lattice fringes, for both particle types, corroborate the crystalline nature of the two phases. The isomeric shift in the Mössbauer spectrum of the CVD deposit, when compared with the Ni_3Sn_4 and SnO_2 standards, confirms the biphasic nature of the obtained material and shows the composition to be Ni_3Sn_4/SnO_2. Electron spectroscopy for chemical analysis (ESCA) studies performed on both (i) as obtained and (ii) argon sputtered samples established the elemental composition, the oxidation states of the Ni and Sn atoms, and the effect of atmospheric oxidation on the metal atoms located on the surface of the layers. Further characterization of the Ni−Sn intermetallic phase was achieved by detailed ESCA and high-resolution transmission electron microscopy (HR-TEM) studies.

Introduction

A considerable amount of progress in materials chemistry has been built upon novel molecular precursors and their reaction chemistry.[1−5] Thin films of new materials prepared by chemical vapor deposition (CVD) show a broad spectrum of properties (e.g, corrosion resistant, dielectric, electrical, magnetic, optical, superconducting, etc.) useful for technolgical development.[6−9] Therefore high-purity metal and oxide films are currently being investigated for several thin film applications.[10] Over the past decade, a substantial amount of work has been carried out on the growth of a variety of metal and oxide films by CVD of suitable molecular precursors; however, the knowledge about the preparation of composite materials by CVD remains elementary.[11−13] Moreover, most of the systems investigated by the molecular precursor route involve just one metallic element, and the multicomponent films have been largely achieved using either a mixture of components or sequential deposition of various components followed by their chemical interaction at the substrate surface. Furthermore, the synthesis of multimetallic systems by the molecular precursor approach remain

* Corresponding author: Fax: 0049-681-302-3995. E-mail: veith@rz.uni-sb.de.

† Institute of Inorganic Chemistry.

‡ Institute of Experimental Physics.

(1) Hampden-Smith, M. J.; Kodas, T. T. *Chem. Vap. Deposition* **1995**, *1*, 1.

(2) Maury, F. *Chem. Vap. Deposition* **1996**, *2*, 113.

(3) Buhro, W. E. *Adv. Mater. Opt. Electron.* **1996**, *6*, 175.

(4) Hubert-Pfalzgraf, L. G. *Appl. Orgamomet. Chem.* **1992**, *6*, 627.

(5) Bradley, D. C. *Chem. Rev.* **1989**, *89*, 1317.

(6) Kodas, T. T.; Hampden-Smith, M. J. *The Chemistry of Metal CVD*; VCH: Weinheim, Germany, 1994.

(7) Pierson, H. O. *Handbook of Chemical Vapour Deposition*; Noyes Publications: Park Ridge, NJ, 1992.

(8) Rees, W. S., Jr. *CVD of Nonmetals*; VCH: Weinheim, Germany, 1996.

(9) Bunshah, R. F. *Handbook of Deposition Technologies for Films and Coatings*; Noyes Publications: Park Ridge, NJ, 1982.

(10) Chopra, K. L.; Major, S.; Panya D. K. *Thin Solid Films* **1983**, *102*, 1.

(11) Meng, G. Y.; Huang, L.; Pan, M.; Chen, C. S.; Peng, D. K. *Mater. Res. Bull.* **1997**, *32*, 385.

(12) Lane, P. A.; Wright, P. J.; Oliver, P. E.; Reeves, C. L.; Pitt, A. D.; Keen, J. M.; Ward, M. C. L.; Tilsley, M. E. G.; Smith, N. A.; Cockayne, B.; Harris I. R. *Chem. Vap. Deposition* **1997**, *3*, 97.

(13) Fischer, R. A. *Chem. Unserer Zeit* **1995**, *29*, 141.

10.1021/cm991034c CCC: $18.00 © 1999 American Chemical Society
Published on Web 10/29/1999

relatively unexplored largely due to the unavailability of suitable precursors.[14−16] In earlier studies, we have demonstrated the potential of chemically driven chemical vapor deposition processes in the synthesis of biphasic composites of the type M/MO_2 (M = Ge, Sn, Pb), Al/Al_2O_3, and $M/M'MO_3$ (M = Ge, Sn, Pb; M′ = Ca, Sr, Ba), where a metallic phase is homogeneously dispersed in a ceramic matrix.[17−20]

Nickel−tin intermetallic compounds with respect to their heat and charge transport properties are finding diverse applications in the electronic industry. Also, Ni−Sn alloys (on silica support) show unique catalytic selectivities in the dehydrogenation of cyclohexane.[21] The alloys for thin film engineering are prepared, in practice, by melting or electrodeposition methods or by the CVD of organotin compounds on Ni/SiO_2 supports; however, in most of the cases a selective synthesis of the desired Ni−Sn phase is difficult, and significant amounts of other phases are invariably formed.[22−24] We report here on the synthesis and characterization of a Ni_3Sn_4/SnO_2 composite in a CVD process using the mixed-metal alkoxide precursor, $[Ni_2Sn_2(O^tBu)_8]$. To our knowledge, there is no report available, so far, on the single source synthesis of an alloy/metal oxide composite via a single source CVD process.

Experimental Section

Synthesis of Nickel Tetrakis(*tert*-butoxy)stannate. The synthesis of the heterometal alkoxide nickel tetrakis(*tert*-butoxy)stannate, $[Ni_2Sn_2(O^tBu)_8]$, was performed as described elsewhere.[25] The product was recrystallized from a *n*-hexane−toluene mixture, at low temperature, and handled using a standard vacuum line and modified Schlenk techniques, taking stringent precautions against atmospheric moisture.

Instrumentation. The CVD experiments were carried out in a horizontal glass tube reactor under reduced pressure. The substrate resting on a quartz carrier was heated inductively by a high-frequency source, and the temperature was monitored by a pyrometer. The whole setup was situated in a heating chamber necessary to promote the volatility of the precursor. The gaseous pyrolysis products formed during the CVD reactions were analyzed with a Hilden analytical HAL quadrupole mass spectrometer, coupled to the CVD assembly. Powder X-ray diffractograms were recorded on a STOE transmission diffractometer system fitted with a SEIFERT X-ray tube operating with Cu Kα (λ = 0.154 18 nm). The powder X-ray diffractograms were visualized with the WIN XPOW software (version 1.01). For the sample preparation, the layers were carefully scratched, ground with a mortar, and filled in a glass capillary. The recording of scanning electron micrographs (SEMs) and the energy-dispersive X-ray (EDX) analysis were performed, under a vacuum, in the specimen chamber of an EDX coupled scanning electron microscope CAM SCAN S4. The TEM images were recorded on a JEM 200 CX transmission electron microscope. High-resolution electron microscopy (HR-TEM) experiments were performed on a PHILIPS CM-200 electron microscope. The X-ray photoelectron spectroscopy (XPS) analyses were performed on a Surface Science Instrument SSI-M-Probe using Al Kα radiation. The Fermi edges of all measurements were calibrated using the Au Fermi edge, and, for the XPS spectra, the Au $4f_{7/2}$ (83.96 eV) core level was used for the calibration of the binding energy. Room temperature Mössbauer spectra were recorded in transmission geometry using a γ ray source (^{57}Co in a rhodium matrix). The stoichiometric Ni−Sn compounds Ni_3Sn, Ni_3Sn_2, and Ni_3Sn_4 were prepared by vacuum induction and electron beam melting.

Results and Discussion

Our earlier investigations[17−20] have shown that the *tert*-butoxides of divalent atoms of group 14 elements, $M(OBu^t)_2$ (M = Ge, Sn, Pb), when subjected to a CVD process disproportionate to yield M/MO_2 composites and volatile byproducts, as illustrated in eq 1.

$$2M(OBu^t)_2 \xrightarrow{\Delta} M^0 + MO_2 + 2Bu^tOH + 2H_2C{=}C(CH_3)_2 \quad (1)$$

With respect to the thermal decomposition behavior, the metal *tert*-butoxides best meet the criteria for ideal precursors. The elimination of the $-OBu^t$ ligands during the CVD process occurs through a clean mechanism since all of the pyrolysis products (*tert*-butyl alcohol, isobutene, and small amounts of dihydrogen) are volatile and can be easily removed from the deposition zone to obtain a ceramic composite with minimum carbon contamination. We have recently reported on the single-source CVD of a novel mixed-metal hydridoalkoxide $[Mg\{AlH_2(O^tBu)_2\}_2]$ which by the virtue of an intramolecular ligand stripping mechanism gave crystalline deposits of nanocrystalline $MgAl_2O_4$ spinel with considerably low carbon contents (<0.5%).[26] The metastable oxidation state of the metallic element plays a key role in the observed decomposition behavior of group 14 *tert*-butoxides, $M^{II}(OBu^t)_2$, where a +2 oxidation state disproportionates to give an elemental (M(0)) phase and a ceramic phase containing the formal M(IV) cation (eq 1). This redox phenomenon has been extended to heterometal alkoxide systems of the general formula $M'M_2(OBu^t)_6$ (M = Ge(II), Sn(II), Pb(II); M′ = Ca, Sr, Ba) which pyrolyze, in a single-source CVD process, to form composites with metallic particles (M(0)) wrapped in a ternary oxide ($M'MO_3$) matrix.[17] In the latter cases, the extraordinary stability of the two-valent atom of the alkaline earth elements leaves them unaffected during the redox process. In view of the above, we were interested in examining the decomposition behavior of a mixed-metal precursor where both metal constituents are prone to redox reactions. Keeping in view the broad range of applications of Ni containing materials, especially in high-density data storage devices and magne-

(14) Veith, M.; Mathur, S.; Mathur, C. *Polyhedron* **1998**, *17*, 1005.
(15) Chandler, C. D.; Roger, C.; Hampden-Smith, M. J. *Chem. Rev.* **1993**, *93*, 1205.
(16) Bradley, D. C. *Polyhedron* **1994**, *13*, 1111.
(17) Veith, M.; Kneip, S. *J. Mater. Sci. Lett.* **1994**, *13*, 335.
(18) Veith, M.; Kneip, S. J.; Jungmann, A.; Hüfner, S. *Z. Anorg. Allg. Chem*. **1997**, *623*, 1507.
(19) Veith, M.; Faber, S.; Hempelman, R.; Janssen, S.; Prewo, J.; Eckerlebe, H. *J. Mater. Sci.* **1996**, *31*, 2009.
(20) Veith, M.; Altherr, A.; Lecerf, N.; Mathur, S.; Valtchev, K.; Fritscher, E. *Nanostruct. Mater.* **1999**, 191.
(21) Onda, A.; Komatsu, T.; Yashima, T. *J. Chem. Soc., Chem. Commun.* **1997**, 1507.
(22) Candy, J. P.; Mansour, A. E.; Ferretti, O. A.; Mablion, G.; Bournonville; Basset, J. M.; Martino, *J. Catal*. **1988**, *112*, 201.
(23) Lesage, P.; Clause, O.; Moral, P.; Didillon, B.; Candy, J. P.; Basset, J. M. *J. Catal*. **1995**, *155*, 238.
(24) Tomishige, K.; Asakura, K.; Iwasawa Y. *J. Catal*. **1994**, *149*, 70.
(25) Veith, M.; Hans, J.; Stahl, L.; May, P.; Huch, V.; Sebald, A. *Z. Naturforsch*. **1991**, *46b*, 403.
(26) Veith, M.; Altherr, A.; Wolfanger, H. *Adv. Mater., CVD* **1999**, *5*, 87.

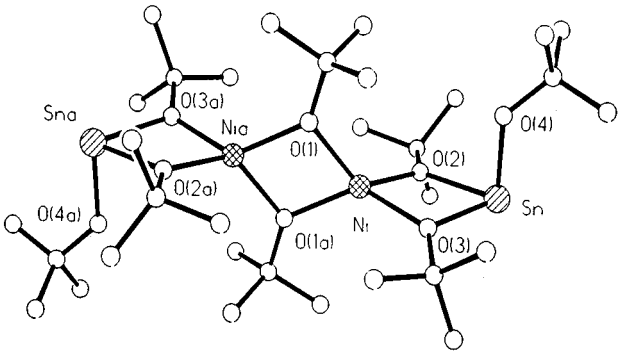

Figure 1. Molecular structure of the mixed-metal precursor $[Ni_2Sn_2(O^tBu)_8]$.[25]

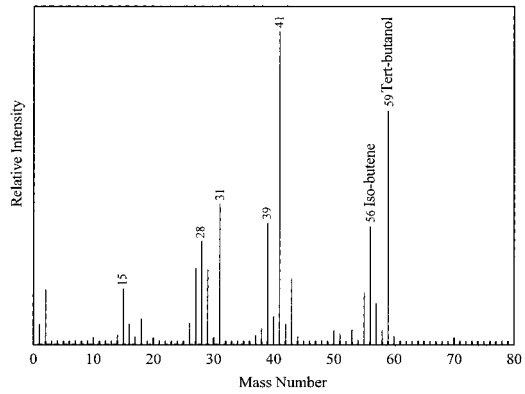

Figure 2. Typical mass spectral pattern observed in the CVD of $[Ni_2Sn_2(O^tBu)_8]$ at 550 °C. The peaks at mass units 56 and 59 represent the characteristic fragments of isobutene and *tert*-butyl alcohol, respectively.

toresistive sensors,[27,28] we have chosen a Ni−Sn heterometal alkoxide, $[Ni_2Sn_2(O^tBu)_8]$, as precursor.[25] The synthesis and structural characterization of $[Ni_2Sn_2(O^tBu)_8]$ have been reported by us. The molecule of empirical formula "$NiSn(OBu^t)_4$" is dimeric in the solid state and exhibits a linear arrangement of four metallic elements (Figure 1).

Chemical Vapor Deposition Process. The chemical vapor deposition of $[Ni_2Sn_2(O^tBu)_8]$ was performed in a cold wall CVD reactor. The apparatus used in the present study works on the technique of vacuum CVD and is similar to the one used by us for the synthesis of other metal/metal oxide composite materials.[17−20] The substrates (steel, copper, silicon wafers) were heated inductively using a high-frequency source. The CVD reactor and the alkoxide reservoir were heated at 120 °C in order to direct the precursor toward the hot (450−550 °C) target. The organic byproducts liberated during the decomposition of the precursor were identified by an on-line mass spectral analysis, which revealed *tert*-butyl alcohol and isobutene as the only volatile fragments (some dihydrogen detected in the mass spectra is a fragmentation product of Bu^tOH and $H_2C{=}C(CH_3)_2$). A representative mass spectrum recorded during the CVD experiment (substrate temperature 550 °C) is shown in Figure 2. For characterization of the decomposition products, the mass spectra of pure Bu^tOH and $H_2C{=}C(CH_3)_2$ were recorded separately, and the observed fragmentaion patterns were successively subtracted from the mass spectra recorded during the CVD process. The peaks remaining at mass numbers 1 and 2, after subtracting the mass spectral features of Bu^tOH and $H_2C{=}C(CH_3)_2$ standard samples, are characteristic of dihydrogen mass spectrum. These observations support the decomposition mechanism of $-OBu^t$ ligands, outlined in eq 1.

Scanning Electron Microscopy and Energy Dispersive X-ray Analysis. The scanning electron micrographs of the films of the Ni_3Sn_4/SnO_2 composite shows a porous surface with a fiberlike consistency. The rate of deposition of the layers could be controlled by varying the experimental parameters (temperature, pressure, precursor flow) and films of different thicknesses ranging between 500 nm and 3 μm were deposited on steel, copper, or silicon wafers. Parts a and b of Figure 3 show the typical surface features of a sample prepared at 550 °C, which exhibit a highly structured morphology and a fibrous growth (Figure 3b).

The energy-dispersive X-ray analysis performed on several spots showed no significant variation in the nickel−tin ratio at the submicrometer level. However, the elemental compositions for various films deposited at 550 °C do not correspond to the Ni:Sn stoichiometry present in the precursor molecule (Ni:Sn = 1:1). The Ni, Sn, and O contents in the films were found to be 7.6(2.0), 32.6(5.0), and 59.8(6.0) at. %, respectively. The elemental mapping (EDX) in a film deposited on a copper substrate (550 °C) shows that both nickel and tin are homogeneously distributed throughout the film (Figure 4a and b). It also reveals that the distribution density is much higher for Sn when compared to Ni. This observation is also supported by the Ni and Sn contents determined by electron spectroscopy for chemical analysis (ESCA) and Mössbauer studies (see later).

Powder Diffraction Studies. A powder X-ray diffractogram of the material deposited at 550 °C is shown in Figure 5. The product, as obtained in the CVD process, is crystalline, and no heat treatment was necessary to identify the phases which were unambiguously indexed[29] as SnO_2 and Ni_3Sn_4 (JCPDS card numbers [21-1250] for SnO_2 and [4-845] for Ni_3Sn_4). The observed XRD patterns were further confirmed by recording the XRD pattern of a standard mixture of Ni_3Sn_4 and SnO_2 and comparing it with the diffractogram observed for the CVD deposit. The crystallite size estimated from the obtained peak profiles using Scherrer's formula[30] gave an average value of 60 and 40 nm for Ni_3Sn_4 and SnO_2 particles, respectively.

X-ray Photoelectron Studies. X-ray photoelectron spectroscopy was used to monitor the elemental composition of the layers and identify the oxidation states of the nickel and tin atoms located on the surface of the layers. Figure 6 shows an overview of the XPS spectrum recorded for a layer prepared at 550 °C. In the case of an unsputtered layer, the presence of carbon is evident as indicated by the C1s peak around 287 eV,[31] which

(27) Fraser, B.; Hampp, A.; Kaesz, H. D. *Chem. Mater.* **1996**, *8*, 1858.
(28) Meng, G. Y.; Huang, L.; Chen, C. S.; Peng, D. K. *Mater. Res. Bull.* **1997**, *32*, 385.
(29) JCPDS Powder Diffraction Data Base, *Joint Committee for Powder Diffraction Standards*, 1990.
(30) Scherrer, P. *Göttinger Nachrichten* **1918**, *2*, 98.
(31) *ESCA Handbook of X-ray Photoelectron Spectroscopy;* Perkin-Elmer Corp.: Eden Prairie, MN, 1992.

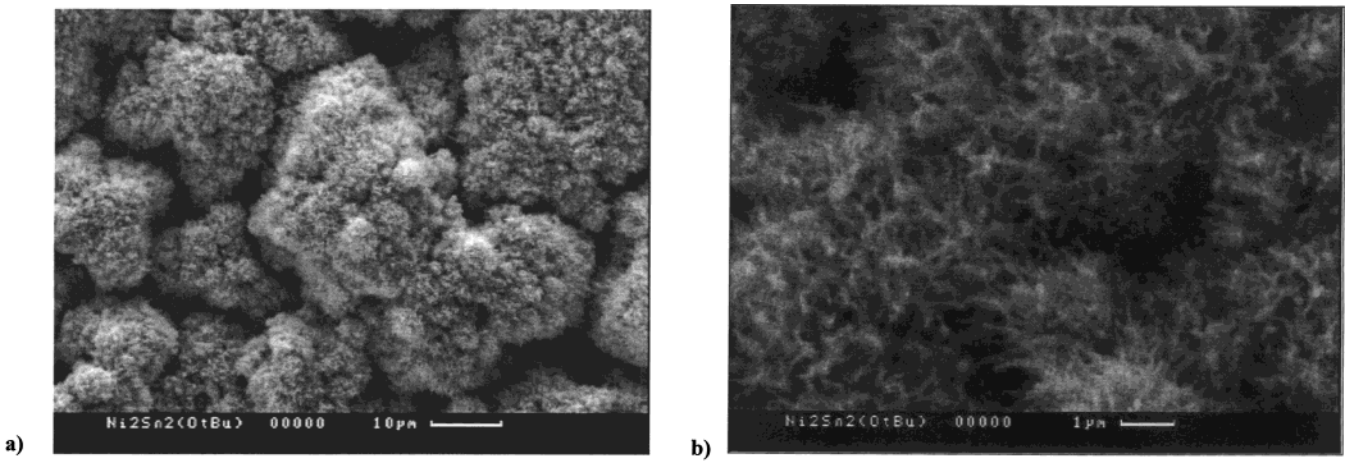

Figure 3. SEM micrographs of the CVD deposit on a copper substrate (550 °C).

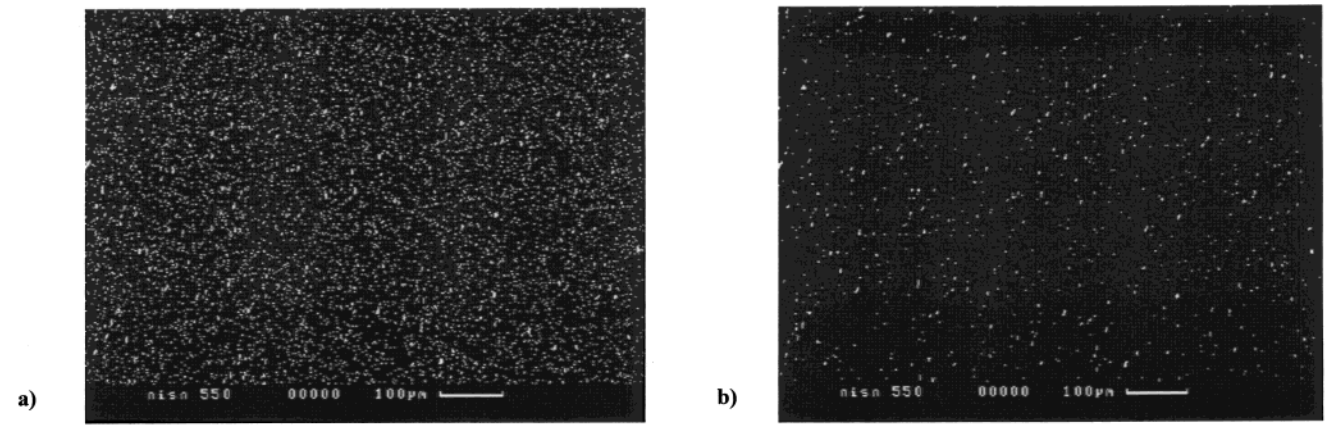

Figure 4. Elemental mapping for tin (a) and nickel (b) in a film deposited on a copper substrate at 550 °C. The distribution density of tin is higher when compared to the nickel distribution.

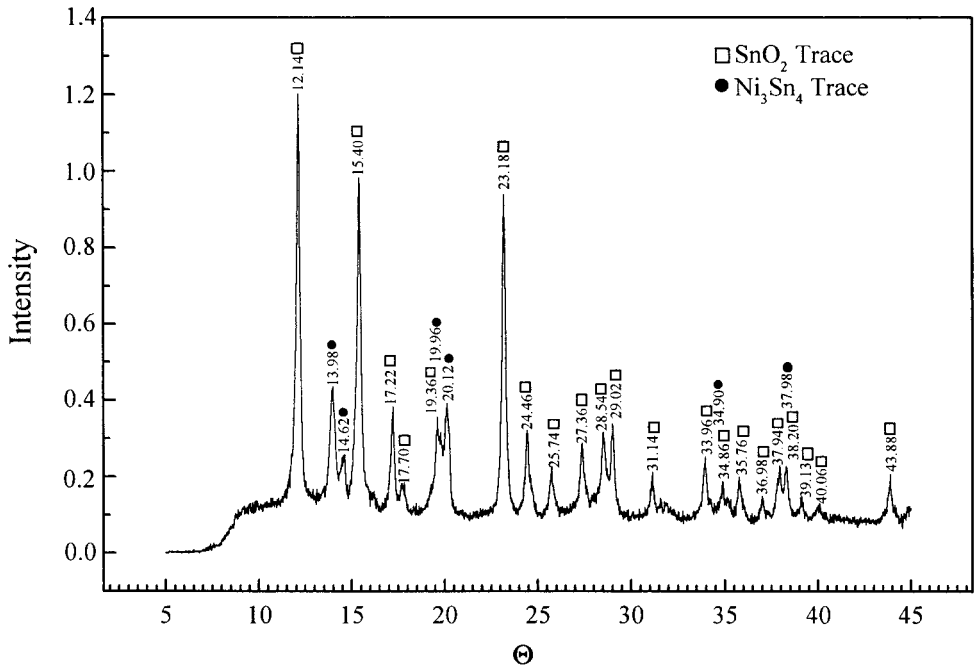

Figure 5. XRD trace of the film material deposited at 550 °C: ●, Ni_3Sn_4 phase (JCPDS file no. [4-845]); □, SnO_2 phase (JCPDS file no. [21-1250]).

results from the CO_2 adsorbed on the surface. The argon sputtering removes the surfacial contamination as observed in the diminished C1s peak (Figure 6b). The adsorption of CO_2 is also evident in the asymmetric nature of the O1s line, where two components (Figure 7) could be fitted, consistent with O1s peaks due to SnO_2 and CO_2.[32] Figure 8 shows the $Sn3d_{5/2}$, $Sn3d_{3/2}$, and O1s peaks observed in the layers deposited at 550 °C and

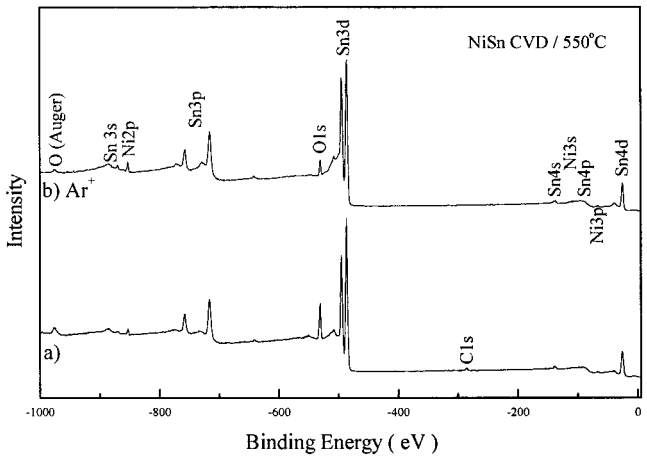

Figure 6. Overview XPS spectra of the film (a) as obtained at 550 °C and (b) after argon sputtering.

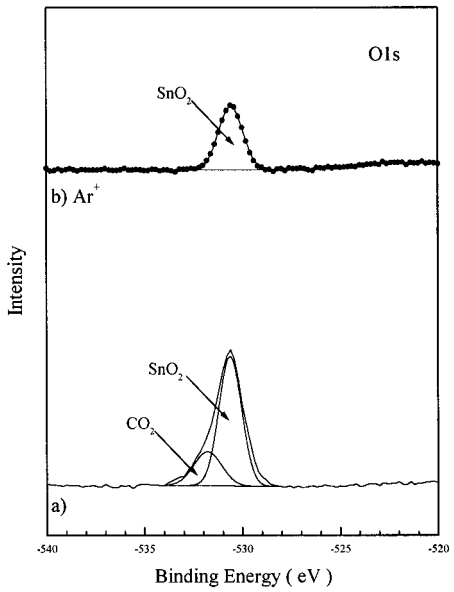

Figure 7. XPS spectra of the O1s band (a) as obtained at 550 °C and (b) after argon sputtering. The surface contamination (adsorbed CO_2) shows large intensity at the high binding energy shoulder of the O 1s peak.

those observed in the reference samples of metallic tin and tin(IV) oxide. It is known that the $Sn3d_{3/2}$ and $Sn3d_{5/2}$ lines are located around 493 and 484.2 eV, respectively, for metallic tin and around 495 and 486.2 eV, respectively, for tin oxide SnO_2.[31,33] The surface of the as obtained layers showed the presence of both Sn(0) and SnO_2 with the Sn:SnO_2 ratio being approximately 20:80. The analyses were performed on both (i) as obtained and (ii) argon sputtered layers, which revealed the atmospheric oxidation of tin atoms located on the surface. The tin content in the layer material was found to increase on sputtering the films, which raised the question of whether the argon sputtering causes the reduction of tin oxide. There is evidence that ion sputtering will result in a change in the chemical composition in the immediate vicinity of the surface.[34]

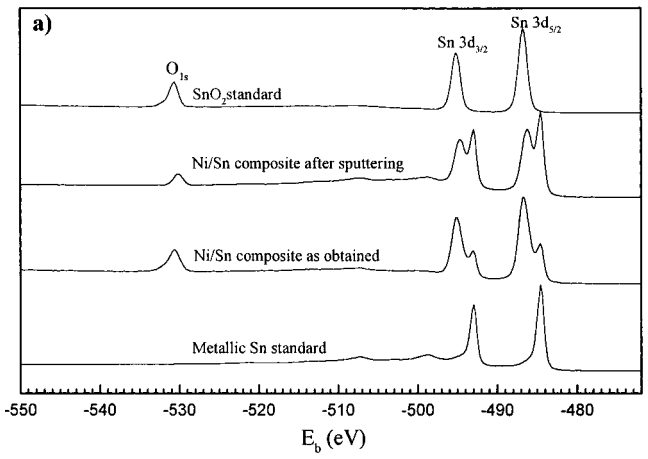

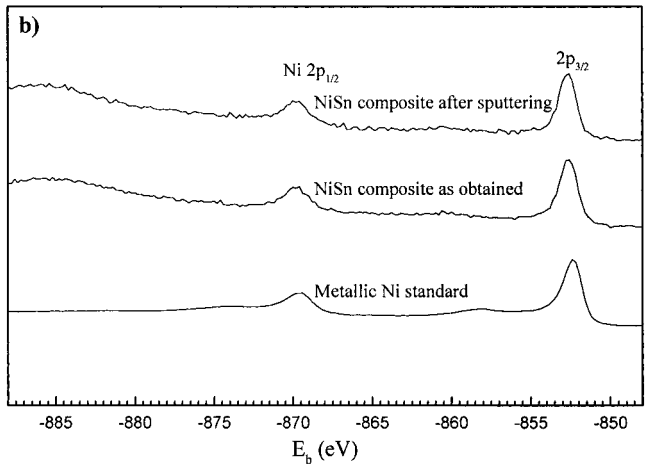

Figure 8. Effect of argon sputtering (4 kV, 3 mA, 8×10^{-8} bar, 15 min) on the Ni (2p) and Sn (3d) bands in the XPS spectra of the film deposited at 550 °C.

To examine the effect of the sputtering process, we have also performed XPS studies on the thin films obtained by the decomposition of $Sn(OBu^t)_2$ and $Sn(OBu^t)_4$, under similar experimental conditions. It is known that tin(II) *tert*-butoxide disproportionates in a CVD process to give a Sn/SnO_2 composite, while only SnO_2 is produced in the decomposition of tin(IV) *tert*-butoxide.[18] The Sn(0):Sn(IV) ratio in the film obtained by the CVD of $Sn(OBu^t)_2$ was found to change on argon sputtering with the peak due to Sn(0) increasing gradually until the Sn(0):Sn(IV) ratio reached a value close to unity. No further increase in the elemental tin content was observed, even after prolonged sputtering, which indicated that no reduction is induced in the film by the argon ions in this experiment and the initial sputtering process merely removed the oxidized layer revealing the actual element ratio (Sn^0:Sn^{IV} = 45:55), formed during the chemical vapor deposition process. This was further confirmed by sputtering the SnO_2 layers, obtained in the CVD of $Sn(OBu^t)_4$, where no Sn(0) could be detected even after long sputtering times. Figure 8b shows a comparison of the XPS spectrum of metallic nickel and that of the CVD deposit prepared at 550 °C. The Ni $2p_{3/2}$ and Ni $2p_{1/2}$ lines characteristic of metallic nickel are found at 852.2 and 870.0 eV, respectively.[31] The position and line shape of the Ni 2p peaks are indicative of the presence of metallic nickel in the CVD product. The argon sputtering showed no effect on the Ni peaks, and the Ni(0) remained unaltered by argon sputtering.

(32) Rossington, D. R.; Condrate, R. A.; Snyder, R. L. *Advances in Material Characterization*; Plenum Press: New York, 1983.
(33) Hüfner, S. *Photoelectron Spectroscopy*; Springer-Verlag: Berlin, 1980.
(34) Fang, C. S.; Pan, F. M.; Tse, W. S.; Horng, S. R. *Surface Sci.* **1989**, *211−212*, 279.

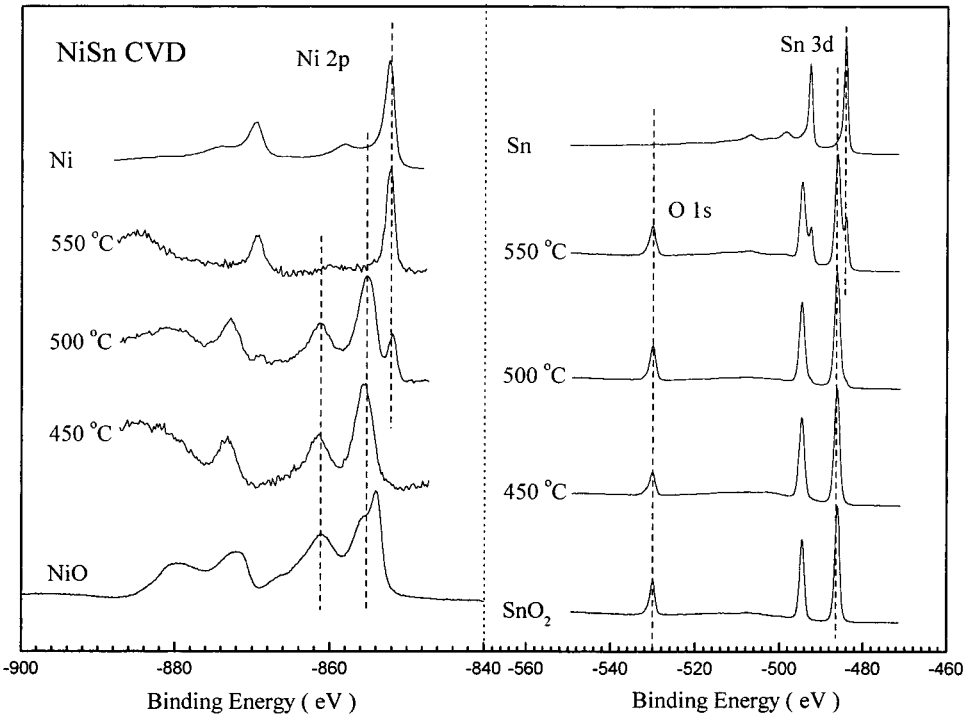

Figure 9. XPS spectra of the films deposited at 450, 500, and 550 °C with reference to elemental Ni and Sn and their oxides (NiO and SnO_2).

The XPS analyses of the films deposited at different temperatures ranging from 450 to 550 °C showed that the obtained composite results from two chemical processes occurring on the substrate surface, namely, (i) disproportionation and decomposition of the precursor (see below) and (ii) redox reactions of nickel and tin species. According to the XPS investigations, the disproportionation of $[Ni_2Sn_2(O^tBu)_8]$ dominates at 450 °C, resulting in the formation of Sn(0), SnO_2, and NiO (Figure 9). Previous studies[18] have shown that the Sn^{II} species disproportionates to give a Sn(0)/SnO_2 composite where Sn(0) particles are embedded in a SnO_2 matrix; the SnO_2 being exclusively situated on the surface is observed at first while Sn(0) wrapped up in the oxide matrix is detected only after argon sputtering. In view of the above, another factor which can contribute to the observed lower content of Sn(0) in nonsputtered films is the surface specific (analyzed depth, 20−50 Å) nature of the ESCA analysis. In this case some of the tin particles which are tightly wrapped in a SnO_2 matrix can remain intact. As a consequence, a higher amount of metallic tin is detected after the sputtering process which removes the oxide shell to show the metallic kernel. At 500 °C, the formation of small amounts of Ni(0) is observed besides Sn(0), SnO_2, and NiO (Figure 9). The redox reactions dominate at 550 °C, where Ni(II) species are totally reduced to Ni(0), which ultimately reacts with elemental tin to form the intermetallic Ni_3Sn_4. The above observations suggest that a redox reaction between NiO and Sn(0) is initiated at 500 °C, which is completed at 550 °C. This assumption is also corroborated by the Ni 2p peak corresponding to NiO, which starts diminishing at 500 °C and disappears at 550 °C (Figure 8).

Since nickel can form three stable intermetallics[35] with tin, namely, Ni_3Sn, Ni_3Sn_2, and Ni_3Sn_4, high-resolution XPS studies were used to rule out the coexistence of any other Ni−Sn phase in the CVD deposit. For this purpose, we have recorded the Ni and Sn core level spectra for the CVD material and have compared the obtained spectra with the spectra recorded for the standard samples of Ni_3Sn_4, Ni_3Sn_2, Ni_3Sn, and Ni. This is shown in the Figure 10a, where the $Ni2p_{3/2}$ band in the CVD product is plotted against the $Ni2p_{3/2}$ lines of Ni_3Sn_4, Ni_3Sn_2, Ni_3Sn, and Ni standards. A closer look at the data reveals that the $Ni2p_{3/2}$ line of the CVD material agrees with the Ni $2p_{3/2}$ line observed in the standard Ni_3Sn_4 sample. The binding energy of the $Ni2p_{3/2}$ line is 852.8 eV in both Ni_3Sn_4 and the CVD product, whereas the binding energy of the $Ni2p_{3/2}$ peak in Ni_3Sn_2, Ni_3Sn, and Ni shows a shift of 0.6 eV (between Ni_3Sn_4 and Ni), which confirms that the only phase present in the CVD product is Ni_3Sn_4 (with respect to the resolution limits of the apparatus). A similar observation is made on comparing the binding energy of $Sn3d_{3/2}$ and $Sn3d_{5/2}$ peaks in the CVD product and Ni_3Sn_4, Ni_3Sn_2, and Ni_3Sn standards (Figure 10b).

Mössbauer Spectroscopy. The ^{119}Sn Mössbauer spectroscopy has been widely used for the identification of the two phases and the quantitative determination of the product compositon.[36−40] In view of the above, the obtained layers were scratched and the ^{119}Sn Mössbauer shifts were measured for the product deposited at 550 °C. Figure 11 shows the ^{119}Sn Mössbauer spectrum of

(35) Nash, P.; Nash, A. *Bull. Alloy Phase Diagrams* **1985**, *6* (4), 1757.
(36) Mildenberger, R.; Venskutonis, A.; Aubertin, F.; Breme, J.; Schwitzgebel, G. *Hyperfine Interact.* **1998**, *112*, 151.
(37) Leidheiser, H.; Czako-Nagy, I.; Varsanyi, M. L.; Vertes, A. *J. Electrochem. Soc.* **1979**, *126*, 204.
(38) Silver, J.; Mackay, C. A.; Donaldson, J. D. *J. Mater. Sci.* **1976**, *11*, 836.
(39) Jaen, J. A.; Varsanyi, M. L.; Csontos, H.; Vertes, A. *Electrochim. Acta* **1990**, *35*, 55.
(40) Varsanyi, M. L.; Jaen, J.; Vertes, A.; Kiss, L. *Electrochim. Acta* **1985**, *30*, 529.

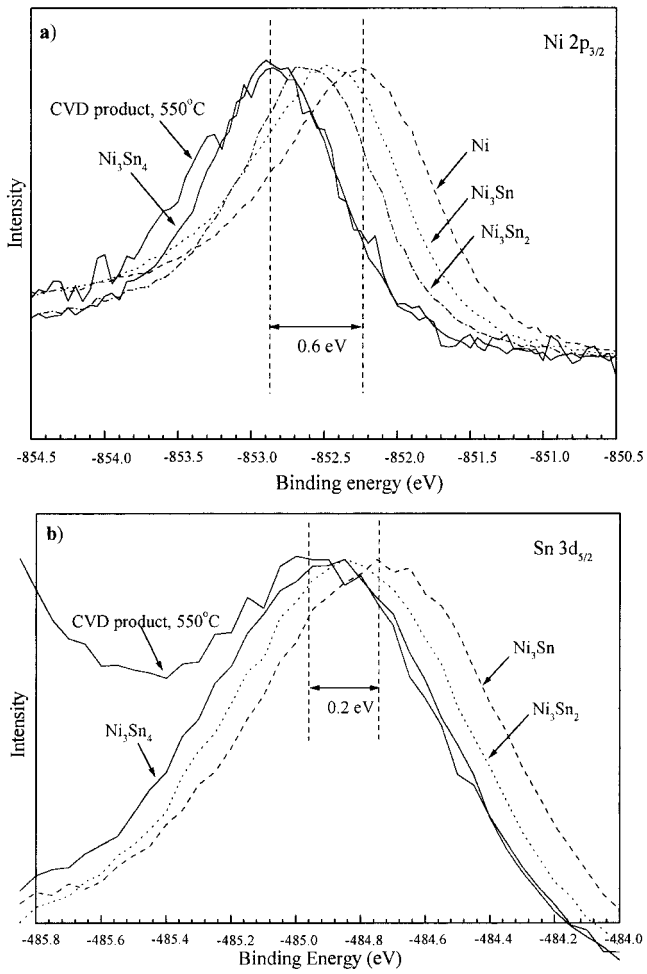

Figure 10. High-resolution XPS spectra ($\Delta E = 0.8$ eV) of the Ni 2p (a) and Sn 3d (b) regions in Ni, Ni_3Sn_4, Ni_3Sn_2, and Ni_3Sn samples. The binding energy values for Ni and Sn in the CVD product are close to the corresponding values in the Ni_3Sn_4 standard.

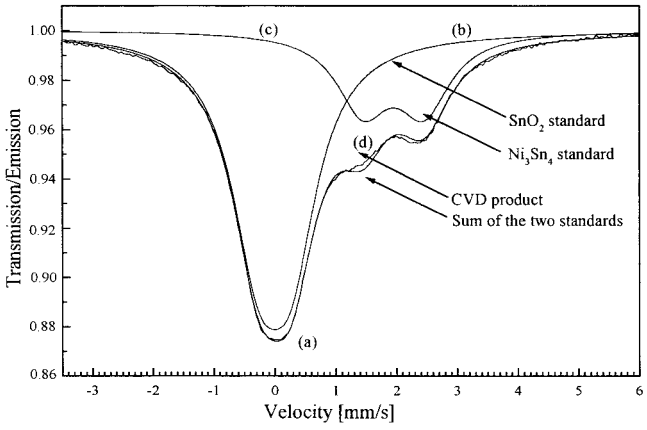

Figure 11. Mössbauer spectra of (a) the CVD product, (b) the SnO_2 standard, (c) the Ni_3Sn_4 standard, and (d) the sum of the two standards (curves b + c).

the CVD product (curve a) plotted with (i) the individual isomeric shifts of SnO_2 (curve b) and Ni_3Sn_4 (curve c) standards and (ii) the summation of shifts due to the two standards (curve d). Interestingly, the curve resulting from the summation of spectra of SnO_2 and Ni_3Sn_4 standards fits well with the spectral pattern observed for the CVD product. A comparison with the curves obtained on adding the spectral features of Ni_3Sn_2/SnO_2 and Ni_3Sn/SnO_2 systems ruled out the possibility of any other Ni−Sn phase being present in the CVD product. A quantitative estimation of the two phases and thus the Ni:Sn ratio in the examined composite could be made using a calibration curve obtained by ^{119}Sn Mössbauer studies on a series of Ni_3Sn_4/SnO_2 samples containing different percentages of Ni_3Sn_4 alloy.[41] The films were found to be composed of 86 mol % SnO_2 and 14 mol % Ni_3Sn_4 with Sn:Ni and Sn(IV):Sn(0) ratios of 3.38 and 1.54, respectively. These observations also illustrate the disproportionation of Sn(II) and a complete reduction of Ni(II) species to elemental nickel, which forms the Ni_3Sn_4 intermetallic compound. It is interesting to note that the ratio between metallic tin and tin oxide as determined by Mössbauer experiments (SnO_2:Sn = 60:40) is higher than that found by ESCA studies (SnO_2:Sn = 55:45). This can be explained in terms of the fact that ESCA is a surface sensitive method, while Mössbauer spectroscopy provides information about the bulk sample that included the surfacially oxidized tin (formed during the grinding of the film material) and the tin oxide matrix (which was partially removed by argon sputtering in the case of ESCA analyses). As a result, the total content of tin(IV) species found by Mössbauer studies is relatively higher than that determined by ESCA.

Transmission Electron Microscopy. A TEM micrograph of the SnO_2/Ni_3Sn_4 composite is shown in Figure 12, which shows a bimodal mixture of crystallites. The composite is made up of nearly spherical particles of size 60−70 nm which are homogeneously dispersed in a matrix of smaller particles (30−45 nm). The bigger size and spherical morphology of the alloy particles, when compared with the crystallite size of tin oxide, is possibly due to the tendency of intermetallic grains to segregate to achieve a globular shape, preferred due to the reduction in the surface energy. The high-resolution transmission electron micrographs of the CVD product show both particle types to be crystalline (Figures 12−14). The lattice parameters of the high-resolution images corresponded to Ni_3Sn_4 (JCPDS [4-845]) and SnO_2 (JCPDS [21-1250]) phases. For measuring the spacing distance (d), the Fourier function transformation (FFT) of the real images was used. The spot EDX analyses of various particles confirmed their chemical composition, as labeled in Figures 13 and 14. The particles are well-dispersed and show developed crystalline phases, as indicated by clear lattice fringes shown in Figures 12 and 13. The HR-TEM image shown in Figure 14 illustrates the presence of the SnO_2 matrix between the two adjacent Ni_3Sn_4 crystallites.

Decomposition Mechanism. In light of various analytical results and the monitoring of CVD products obtained in the temperature range 450−550 °C, it is evident that the target temperature plays a decisive role in determining the course of the reaction and thus the nature of the decomposition products (Chart 1). The ESCA studies on the films deposited at different temperatures (Figure 9) indicate that two chemical processes are active during the CVD process: (i) fragmentation of the molecular precursor to generate Sn(0),

(41) Venskutonis, A.; Aubertin, F.; Breme, J. Results to be published.

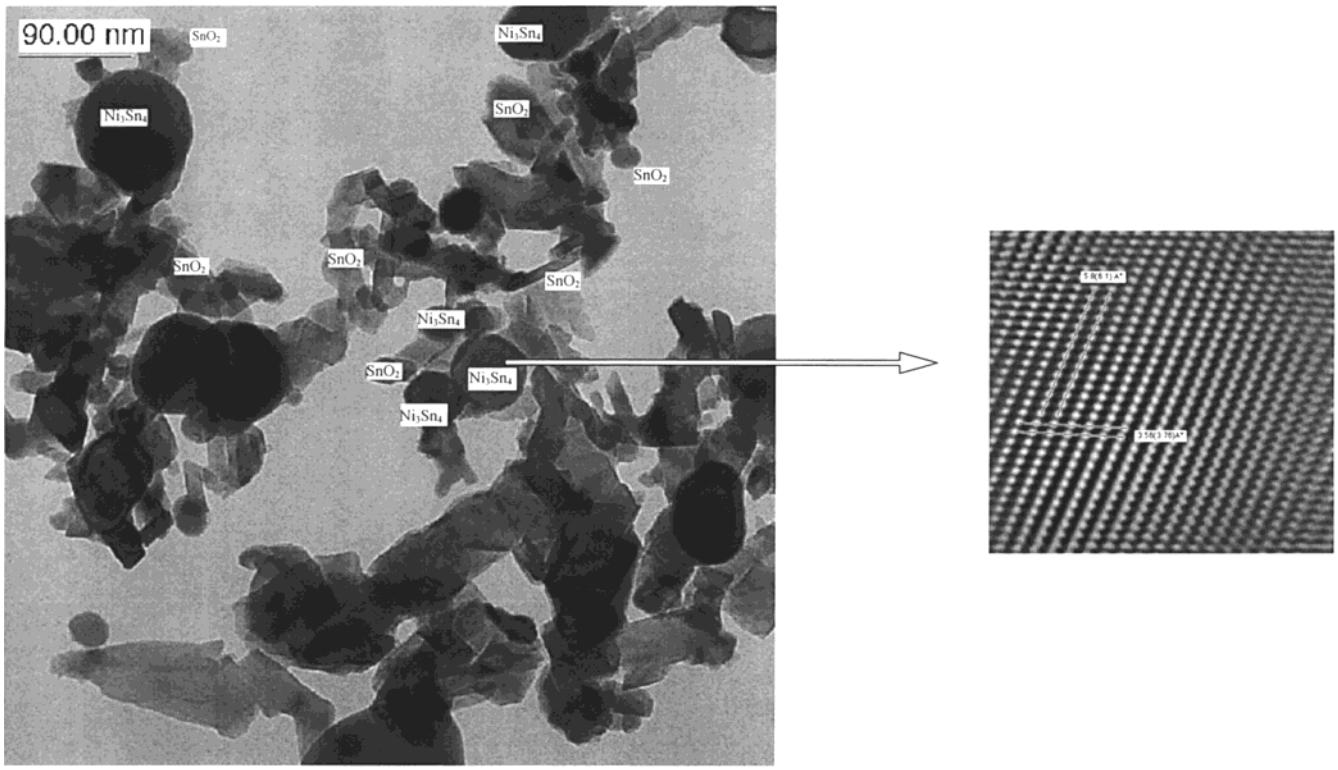

Figure 12. HR-TEM image of Ni_3Sn_4/SnO_2 composite and FFT image of a Ni_3Sn_4 grain. The lattice parameters correspond to intermetallic Ni_3Sn_4 (JCPDS [4-845]).

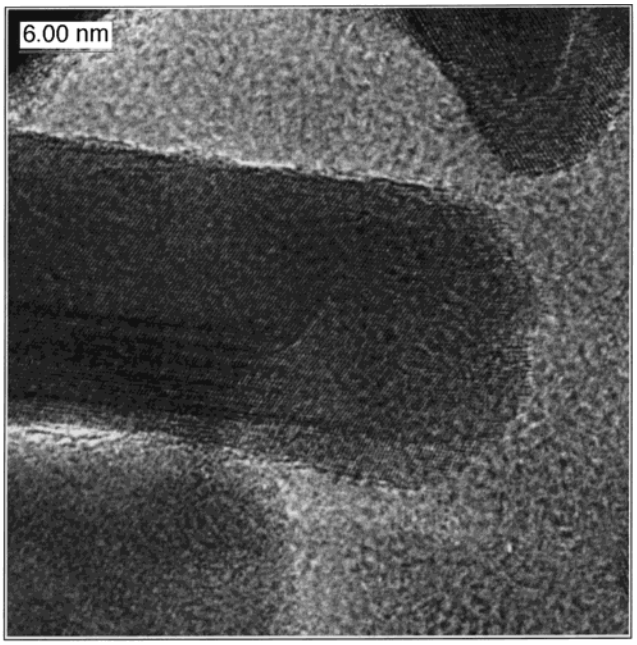

Figure 13. HR-TEM image of a SnO_2 crystallite.

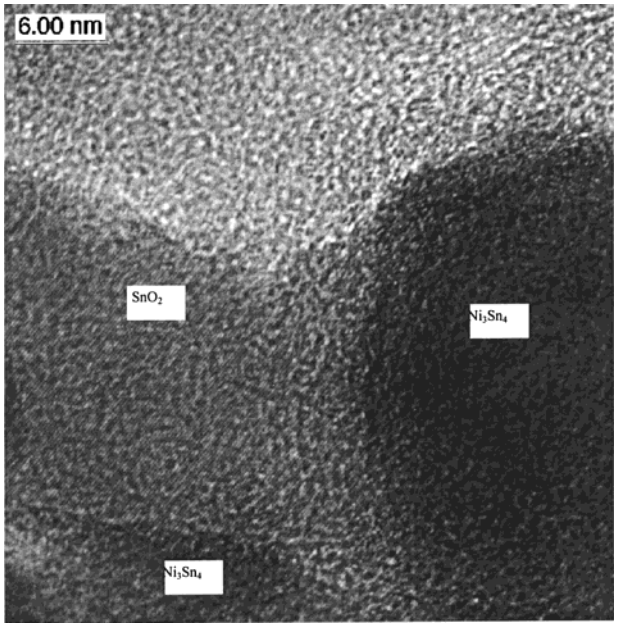

Figure 14. HR-TEM micrograph of the composite showing the SnO_2 matrix between two Ni_3Sn_4 crystallites.

SnO_2, and NiO and (ii) the redox reaction between NiO and Sn when Ni(II) is reduced to elemental nickel which forms the intermetallic Ni_3Sn_4 with tin formed in the first process (Chart 1).

The first decomposition process takes place below 500 °C and involves the fragmentation of the precursor molecule in the gas phase to produce Ni(II) and Sn(II) species, which decompose on the heated target surface to produce NiO, Sn, and SnO_2 (Scheme 1). Note that 500 °C is sufficiently high temperature for the complete disproportionation of Sn(II) species to produce the Sn/SnO_2 composite.[18] The second process occurs on the target surface and involves a redox reaction between Ni and Sn containing species to produce Ni_3Sn_4 alloy (Scheme 1). The above findings together with the observed low Ni content (Ni, 12%; Sn, 40%; O, 48%) suggest that the volatility of the precursor $[Ni_2Sn_2(O^tBu)_8]$ is insufficient and is hampered by a partial thermal disproportionation of the heterometal framework. The fragmentation process would ideally generate an equimolar mixture of $Ni(OBu^t)_2$ and $Sn(OBu^t)_2$; however, the Ni:Sn ratio in the obtained composite deviates from the intended 1:1 stoichiometry. Apparently, a partial fragmentation of $[Ni_2Sn_2(O^tBu)_8]$ in

Scheme 1

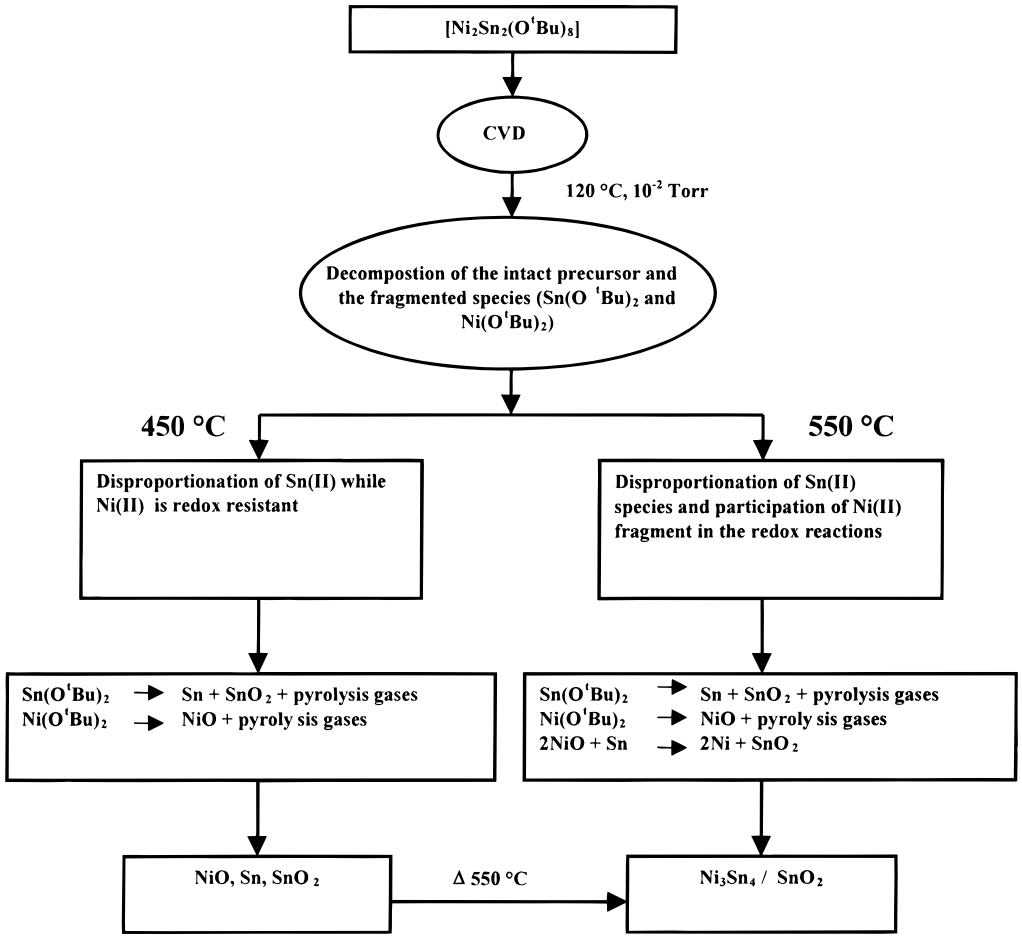

Chart 1

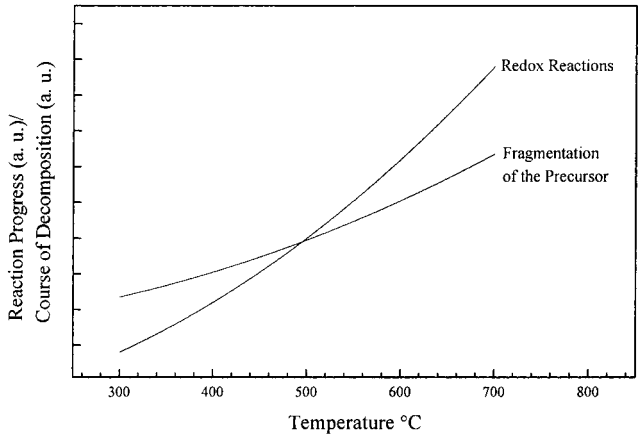

$Ni(OBu^t)_2$ and $Sn(OBu^t)_2$ occurs already in the precursor reservoir.

This was supported by elemental analysis of the product left in the flask, after the CVD process, which showed a Ni-rich residue (Ni content: 35.60%; calcd for $[Ni_2Sn_2(O^tBu)_8]$, 22.65%; calcd for $[Ni(OBu^t)_2]_n$, 57.27%). Due to the high volatility, the fragmented tin(II) *tert*-butoxide is completely transported into the gas phase, whereas nickel *tert*-butoxide being nonvolatile is left in the flask which is responsible for the observed high tin content in the films. In view of the above, the only source of Ni in the films is the fraction (ca. 30%) of undecomposed $[Ni_2Sn_2(O^tBu)_8]$ (determined from the composition of the CVD deposit and the elemental analysis of the product left in the flask after the CVD experiment) which had been transported intact into the gas phase. In summary, the formation of a Ni_3Sn_4/SnO_2 composite which differs, in terms of the Ni:Sn ratio, from the starting material can be understood according to the following equilibrium presumably active during the transport of precursor in the gas phase:

$$(1/2)[Ni_2Sn_2(O^tBu)_8] \rightleftharpoons (1/2)[Sn(OBu^t)_2]_2 + (1/n)[Ni(OBu^t)_2]_n$$

Conclusion

Use of $[Ni_2Sn_2(O^tBu)_8]$ as a single-source precursor in a CVD process offers, under distinct conditions, nanoscaled composite where an intermetallic compound (Ni_3Sn_4) is uniformly dispersed in an oxide (SnO_2) phase. The chemically controlled decomposition of the mixed-metal precursor is responsible for the homogeneous distribution of one phase into another and demonstrates the potential of the molecular precursor approach in obtaining new types of ceramic matrix composites. Another noteworthy feature of the present study is the low temperature (550 °C) of formation of an intermetallic compound composed of a high (Ni, 1453 °C) and a low (Sn, 232 °C) melting component. The present study also throws light on the prerequisites of molecular precursors with respect to a CVD process. The various factors such as fragmentation, volatility of the

constituent fragments, gas-phase equilibria, decomposition behavior, and temperature of the components, etc., can play a dominating role in determining the fate of the final material.

The results obtained suggest that the molecular precursor, $[Ni_2Sn_2(O^tBu)_8]$, exhibits a limited volatility and decomposes partially in the gas phase to yield the constituting Ni(II) and Sn(II) *tert*-butoxides. Nevertheless, a significant amount of the precursor is transported intact to the deposition zone, resulting in the formation of the Ni_3Sn_4/SnO_2 composite. The fragmentation of the heterometal framework allows the volatile tin(II) *tert*-butoxide molecules to reach the substrate surface, while the nonvolatile nickel(II) *tert*-butoxide is left in the flask. The Ni-rich residue, left in the flask after the CVD experiment, together with the higher tin contents in the CVD deposits supports the above argument.

Acknowledgment. The authors gratefully acknowledge the financial support of the Deutsche Forschungsgemeinschaft in the framework of the research program *Sonderforschungsbereich 277* at the University of Saarland, Saarbruecken. M.V. thanks the Fonds der Chemischen Industrie for their generous support. We thank Prof. J. Breme and A. Venskutonis for recording the Moessbauer spectra. Thanks are also due to Dr. T. Kraweski and Dr. M. Jillavi for transmission electron microscopy experiments.

CM991034C